Opto-Electronic Advances

Supplementary information

2020, Vol. 3, No. 8

DOI: 10.29026/oea.2020.200004

Fresnel incoherent correlation holography with single camera shot

Anand Vijayakumar[1]*, Tomas Katkus[1], Stefan Lundgaard[1], Denver P. Linklater[1,2], Elena P. Ivanova[2], Soon Hock Ng[1] and Saulius Juodkazis[1,3,4]*

[1] Optical Sciences Centre and ARC Training Centre in Surface Engineering for Advanced Materials (SEAM), School of Science, Swinburne University of Technology, Hawthorn 3122, Australia. [2]Department of Physics, Royal Melbourne Institute of Technology, GPO Box 2476, Melbourne 3001, Australia. [3]Melbourne Centre for Nanofabrication, Australian National Fabrication Facility, 151 Wellington Road, Clayton 3168, Australia. [4]Tokyo Tech World Research Hub Initiative (WRHI), School of Materials and Chemical Technology, Tokyo Institute of Technology, 2-12-1, Ookayama, Meguro-ku, Tokyo 152-8550, Japan.

*Correspondence: A Vijayakumar, E-mail: vanand@swin.edu.au; S Juodkazis, E-mail: sjuodkazis@swin.edu.au

This file includes:

Supplementary information for this paper is available at https://doi.org/10.29026/oea.2020.200004

Section 1: Working principle of FINCH and conditions for achieving super-resolution

The working principle of FINCH is briefly explained using Fig. S1. A point object is located on the optical axis at z_0 from a dual-lens system with focal lengths f_1 and f_2. The dual-lens creates two mutually coherent waves and two-point images at $z_1 = (1/f_1 - 1/z_0)^{-1}$ and $z_2 = (1/f_2 - 1/z_0)^{-1}$ from the dual-lens. An image sensor is located at $(z_1+z_2)/2$ from the dual-lens, where the two mutually coherent waves are perfectly overlapped. The complex amplitude of the two interfering waves can be represented as $C_1Q(1/Z)$ and $C_2Q(-1/Z)$, where C_1 and C_2 are complex constants and $Q(1/Z) = \exp[j\pi r^2/(\lambda Z)]$, where $Z=(z_2-z_1)/2$. The interference between the two mutually coherent waves, $I_{\mathrm{PSH}} = \{C_1Q(1/Z) + C_1Q(-1/Z)\}^2$ results in a circular fringe pattern with a spatial frequency twice that of the quadratic phase $Q(1/Z)$. This self-interference pattern is also the point spread hologram (PSH) of the FINCH system. Considering a spatially incoherent illumination, a complicated object can be considered as a collection of independent point objects expressed as $o(\overline{r}_o) = \sum_{i=1}^{M} a_i \delta(r - r_i)$. A circular fringe pattern is obtained for every object point and is added in the sensor plane, unlike coherent illumination where there is an interference between the two complex amplitudes. The object intensity pattern can be therefore expressed as $I_o = \sum_{i=1}^{M} a_i I_{\mathrm{PSH}} \otimes \delta(r - r_i)$ which when propagated numerically to one of the images planes reconstructs the object, where '$\otimes$' is a 2D convolutional operator. The twin image and bias terms present in this inline hologram are removed by propagating a complex hologram generated by the superposition of at least three phase-shifted holograms to one of the image planes. Alternatively, the image of the object can be reconstructed by a cross-correlation between the object hologram and the PSH $I = I_{\mathrm{PSH}} * I_o$.

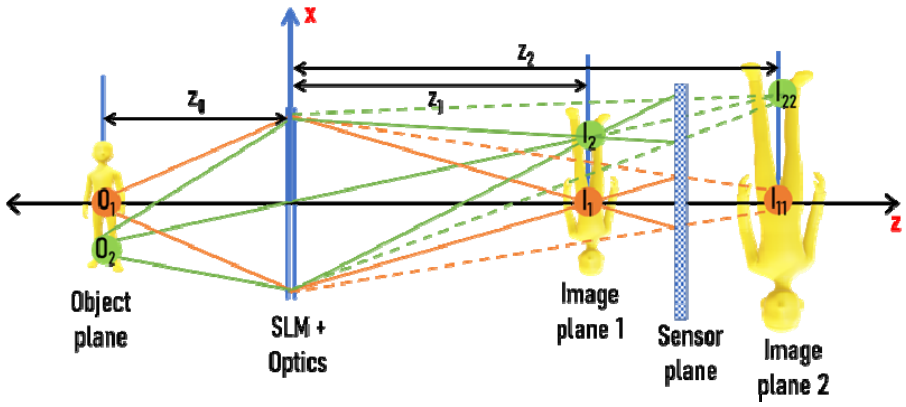

Fig. S1 | Optical configuration of FINCH for resolution enhancement. (Dotted lines indicate the image formation at the second image plane)

As per the above description, FINCH seems like a regular incoherent imaging system. However, the two-point resolution of FINCH is different from a classical system, resulting in the super-resolution capability. In a regular imaging system, when two object points which are separated by a distance are imaged, the magnification of the point is equal to the magnification of the spacing between the points in the image plane. This is called as Lagrange invariant or Smith-Helmholtz Invariant condition. In FINCH, the magnification of the spacing between the points can be different from that of the magnification of the point itself depending upon the optical configuration of FINCH resulting in an imaging resolution different from that of the regular imaging system. The modified Lagrange invariant conditions for FINCH have been studied in detail. Let us consider the optical configuration for achieving maximum super-resolution conditions in FINCH, i.e. when the magnification of the spacing between the two points is twice as much as the magnification of the points. Two points are imaged using the FINCH imaging system, where one point is present on the optical axis while the other is not as shown in Fig. S1. The FINCH system produces two images for the two object points at two axial planes corresponding to the focal lengths of the two lens functions. FINCH uses a spatially incoherent light and therefore there is no interference between two different points in the object, but only self-interference between two points generated from the same point. Therefore, the waves emanating from object points O_1 and O_2 do not interfere with each other but only with themselves.

Two image points I_1 and I_{11}, and I_2 and I_{22} are generated at two planes corresponding to the two object points O_1 and O_2 respectively. In the sensor plane, the hologram is obtained by interference between the two points I_1 and I_{11} added to the interference between the two points I_2 and I_{22}. The waves emanating from points I_1 and I_{11} have equal and opposite quadratic phase factors given by $Q(1/Z)$ and $Q(-1/Z)$ respectively. The waves from points I_2 and I_{22} have equal and opposite quadratic phase factors respectively as I_1 and I_{11} but in addition, the points also have linear phase factors given by $L(\overline{o}/Z)=\exp[\mathrm{j}2\pi(o_x x)/(\lambda Z)]$ with opposite signs. When the two beams are perfectly overlapped, the two equal and opposite linear phases add up resulting in a linear phase given by $\exp[\mathrm{j}4\pi(o_x x)/(\lambda Z)]$. During reconstruction involving a numerical propagation to one of the image planes, the acquired larger linear phase moves the two points laterally farther from one another while the size of each spot remains a constant resulting in an overall lateral resolution enhancement.

It is seen from the above analysis that the super resolution exists only in a particular object plane that results in a perfect overlap between the two beams in the sensor plane. Any change in the location of that object plane disrupts the beam overlap condition and the maximum resolution of FINCH could not be obtained. Therefore, to image multiple planes of a thick object using FINCH, it is necessary to mechanically shift the location of the object every time to match that particular plane to the beam overlap condition.

Section 2: Aberration correction and random multiplexing procedure for RMBDL

The randomly multiplexed FZLs will be fabricated on a glass substrate. Earlier studies indicated that the exclusion of the thickness and the refractive index of glass plates introduces substantial spherical aberration into the system resulting in a variation in the focal distances and blurring of the focal spot. Two techniques have been proposed to avoid spherical aberration. In the first technique, the glass substrate was included in the calculation of the zones of the FZL. In the second case, an equivalent and opposite aberration were introduced during fabrication to compensate for the spherical aberration. Considering the higher success with the first method, it is adapted for this design. For a thickness t and refractive index n_g of the glass substrate, the phase of the glass substrate is given as $\phi_G = 2\pi n_g t/\lambda$. The phases of two FZLs after the inclusion of the substrate correction are given as $\phi'_{FZL1} = -(\pi r^2/\lambda z_1) - (2\pi n_g t/\lambda)$ and $\phi_{FZL2} = -(4\pi r^2/\lambda z_2) - (2\pi n_g t/\lambda)$. A random phase function ϕ_r with a predefined scattering ratio is synthesized using Gerchberg-Saxton algorithm (GSA) and binarized to two levels as $M = \text{round}(\phi_r/2\pi)$. An inverted image of M given as 1–M is synthesized next. The RMBDL is designed by randomly multiplexing the two FZLs using the random phase functions as

$$\phi_{RMBDL} = [-(4\pi r^2/\lambda z_2) - (2\pi n_g t/\lambda)]M + [-(\pi r^2/\lambda z_1) - (2\pi n_g t/\lambda)](1-M) \quad . \tag{S1}$$

The RMBDL was designed for z_1 = 5 cm, z_2 = 10 cm, λ = 617 nm, diameter of the FZLs D = 5 mm, t = 1.1 mm, n_g = 1.5 for ITO coated glass plates. The images of the FZLs before and after the substrate correction, GSA algorithm for random matrix synthesis and the synthesis of RMBDL with random multiplexing are shown in Fig. S2. A scattering ratio of σ = b/B = 0.1 was selected and iterated 50 times. The final RMBDL was binarized to two levels for ease of fabrication as shown in Fig. S2. The binarization step may result in the generation of multiple diffraction orders and for analysis in the next section, the contribution in the first diffraction order is only considered while the other orders are negligible in comparison to the first diffraction order. The magnification of the system at $z_2/2$ from the RMBDL is 1.

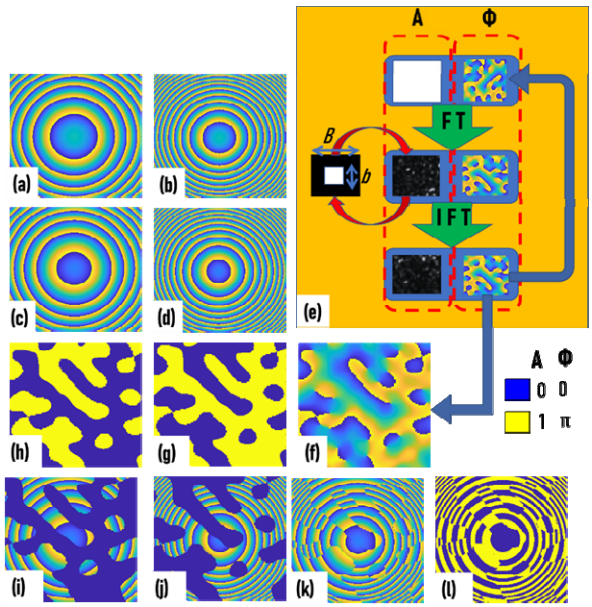

Fig. S2 | Procedure for designing RMBDL. Phase images of the FZL$_1$ (**a**) before and (**c**) after **aberration compensation. Phase images of FZL$_2$** (**b**) before and (**d**) after aberration compensation. (**e**) GSA for synthesizing a phase mask with a scattering ratio of b/B. (**f**) Phase mask synthesized from GSA. (**g**) Binary phase mask after binarization to two levels. (**h**) Inverted image of the phase mask. Phase images of (**i**) FZL$_1$ and (**j**) FZL$_2$ after multiplying the binary phase mask. Phase images of RMBDL (**k**) before and (**l**) after binarization to two levels.

Section 3: Comparison of different decorrelation techniques

FINCH with a polarization multiplexing scheme where all the SLM pixels were utilized for the generation of the two beams is compared with a random multiplexing scheme with different scattering ratio masks using the recently developed non-linear correlation technique. The above FINCH cases were also studied using well-established decorrelation methods such as the Lucy-Richardson method, Weiner Filter and Fresnel backpropagation. The design values described in Supplementary Section 2 are used for simulation and Swinburne University's emblem has been used as a test object. The images of the point object holograms and object holograms for the above FINCH cases are shown in Fig. S3. The reconstruction results using the Lucy-Richardson method, Weiner Filter, Fresnel backpropagation and non-linear filter with minimum entropy are shown in Fig. S3. From the reconstruction results, it is seen that Fresnel propagation means of reconstruction is not successful due to the presence of twin image and bias terms. Non-linear reconstruction method reconstructed the image but it is noisy. Lucy-Richardson algorithm needed about 200 iterations with the 'deconvlucy' function of MATLAB to reconstruct the image, but the reconstructed image was blurred and the time consumed was 120 seconds (Intel core i5-8250U CPU 1.6 GHz, 1.8 GHz, 8 Gigabytes RAM).

Therefore, the Lucy-Richardson algorithm may not be ideal for real-time three-dimensional imaging but can be used to record events for later analysis. Another observation in the results of the Lucy-Richardson algorithm is that with a decrease in the scattering ratio, the blur in the reconstructed results appears to increase. Weiner filter produced results identical to that of the image. However, previous studies on Weiner filter under non-ideal noisy configurations showed a lower SNR. From the study, it is seen that the scattering ratio does not have much effect on the reconstruction results. A higher scattering ratio increases the computational data and the size of the CAD file. The design was generated with a scattering ratio $\sigma = 0.1$ and a diameter of 5 mm as a bitmap file and converted into GDSII format using the trial version of LinkCAD software. The file size was approximately 65 Megabytes.

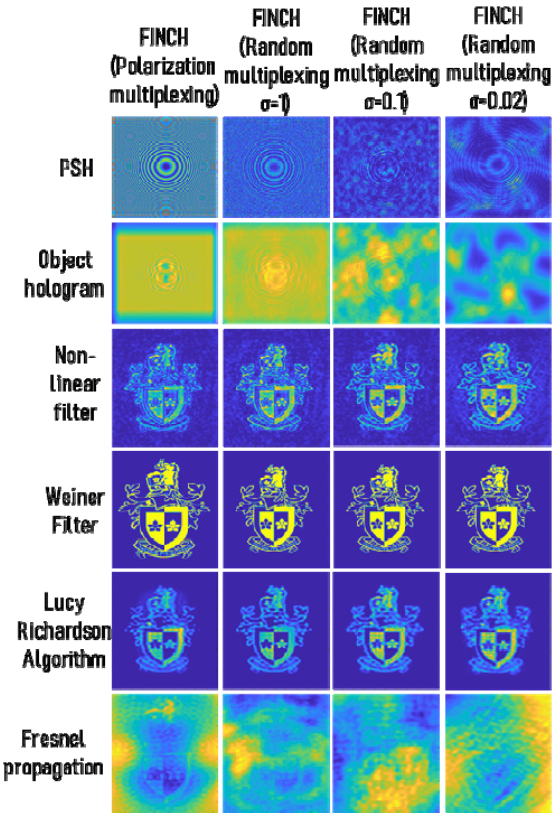

Fig. S3 | Reconstruction results of FINCH in different configurations using different decorrelation techniques such as non-linear filter, Weiner filter, Lucy-Richardson filter (200 iterations) and Fresnel propagation.

Section 4: Reconstruction by the non-linear filter

The values of α and β were varied in steps of 0.2 from -1 to +1 and a low pass filter and median filter were implemented simultaneously and the entropy was calculated for each case. The reconstruction results of the USAF object is shown in Fig. S4. The reconstruction results for negative values of α did not produce any result.

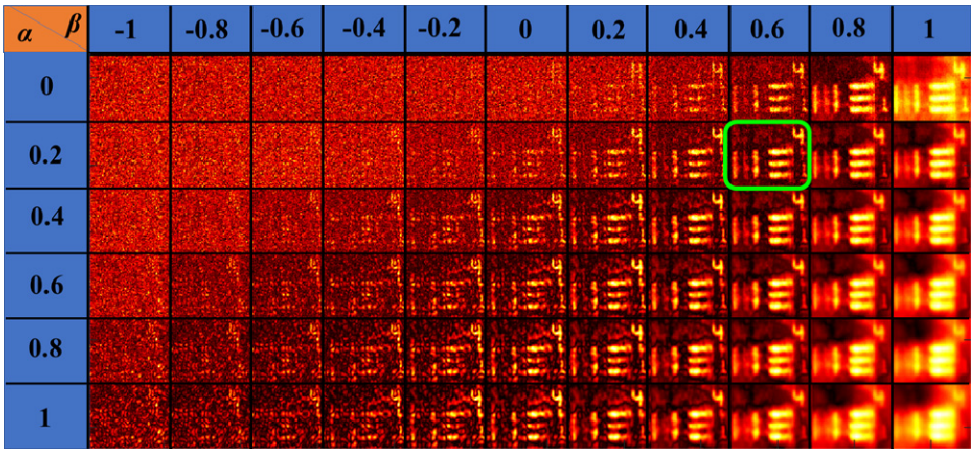

Fig. S4 | Reconstruction results using the non-linear filter for different values of α and β. The result with the lowest entropy is indicated by a green box.